PAPER

Coherent cancellation of photothermal noise in GaAs/Al$_{0.92}$Ga$_{0.08}$As Bragg mirrors

View the article online for updates and enhancements.

Coherent cancellation of photothermal noise in GaAs/Al$_{0.92}$Ga$_{0.08}$As Bragg mirrors

Tara Chalermsongsak[1]**, Evan D Hall**[1]**, Garrett D Cole**[2,3]**, David Follman**[2]**, Frank Seifert**[4]**, Koji Arai**[1]**, Eric K Gustafson**[1]**, Joshua R Smith**[5]**, Markus Aspelmeyer**[6] **and Rana X Adhikari**[1]

[1] LIGO Laboratory, California Institute of Technology, MS 100–36, Pasadena, CA 91125, USA
[2] Crystalline Mirror Solutions LLC, 114 E Haley, Suite G, Santa Barbara, CA 93101, USA
[3] Crystalline Mirror Solutions GmbH, Parkring 10, A–1220 Vienna, Austria
[4] Joint Quantum Institute, National Institute of Standards and Technology and University of Maryland, 100 Bureau Drive, Gaithersburg, MD 20899, USA
[5] Department of Physics, California State University Fullerton, Fullerton, CA 92831, USA
[6] Vienna Center for Quantum Science and Technology (VCQ), Faculty of Physics, University of Vienna, A–1090 Vienna, Austria

E-mail: ehall@caltech.edu

CrossMark

Abstract

Thermal noise is a limiting factor in many high-precision optical experiments. A search is underway for novel optical materials with reduced thermal noise. One such pair of materials, gallium arsenide and aluminum-alloyed gallium arsenide (collectively referred to as AlGaAs), shows promise for its low Brownian noise when compared to conventional materials such as silica and tantala. However, AlGaAs has the potential to produce a high level of thermo-optic noise. We have fabricated a set of AlGaAs crystalline coatings, transferred to fused silica substrates, whose layer structure has been optimized to reduce thermo-optic noise by inducing coherent cancellation of the thermoelastic and thermorefractive effects. By measuring the photothermal transfer function of these mirrors, we find evidence that this optimization has been successful.

(Some figures may appear in colour only in the online journal)

1. Introduction

Many precision optical experiments, such as Advanced LIGO [1], employ free-space Fabry–Pérot optical cavities formed from high-performance Bragg mirrors. Much effort has been put into improving the frequency stability of these optical cavities. This has involved work on laser frequency stabilization, laser power stabilization (in the audio band and at radio frequencies [2]), vibration isolation [3–5], and temperature stabilization [5]. Within the last fifteen years, this work has led to optical cavities whose frequency stability is limited by thermal noise in the high-reflectivity mirror coatings. In the case of Advanced LIGO, these coatings are multilayer stacks of ion-beam-sputtered silica (SiO$_2$) and titania-doped tantala

(Ti: Ta$_2$O$_5$) [6]. Experimental investigation has revealed that thermal noise in SiO$_2$/ Ta$_2$O$_5$ coatings is dominated by mechanical loss in the tantala layers [7]. This loss is usually a few parts in 10^4 for undoped coatings, and the addition of titania dopant can reduce this loss by at most a factor of two [8].

In the quest for ever more stable Fabry–Pérot cavities, several groups have looked for ways of reducing thermal noise below the limit set by quarter-wavelength (QWL) silica/tantala stacks [9–11]. In particular, Cole *et al* [12] fabricated Bragg mirrors from single-crystal QWL stacks of gallium arsenide (GaAs) and aluminum-alloyed gallium arsenide (Al$_x$Ga$_{1-x}$As) via a substrate transfer and direct bonding technique. With these mirrors, they formed an optical cavity whose frequency noise is below the silica/tantala thermal noise level in the band

from 1 to 10 Hz, and is consistent with a loss angle below 4×10^{-5}, an order of magnitude lower than the dissipation in silica/tantala Bragg mirrors. Independent ringdown measurements on micromechanical AlGaAs resonators by Cole *et al* [13, 14] confirm this, with measured loss angles as low as 2.4×10^{-5} at room temperature [15].

AlGaAs has been used for nearly 40 years in optical interference coatings [16, 17], and so its mechanical and optical properties have been well characterized. This makes AlGaAs an attractive coating candidate, since its thermal noise performance at room temperature can be accurately modeled.

While AlGaAs is expected to produce lower Brownian noise than silica/tantala (owing to its lower mechanical dissipation), it has the potential to produce greater thermo-optic noise because the values of the linear coefficient of thermal expansion (CTE) $\alpha = (1/L)\partial L/\partial T$ and coefficient of thermorefraction (CTR) $\beta = \partial n/\partial T$ are higher in AlGaAs than in silica/tantala. Coherent cancellation of thermal noise has been described [18–20] for both Brownian noise and thermo-optic noise (driven by temperature fluctuations) by carefully optimizing the coating's layer structure. We have carried out such an optimization, with the goal of not only minimizing thermo-optic noise, but also controlling the amplitude transmissivity and reflection phase.

2. Theory of thermal noise

For a Fabry–Pérot cavity whose mirror surfaces are interrogated by a laser beam, we consider thermal noise terms arising from either mechanical loss or thermal dissipation. These mechanisms lead to Brownian noise and thermo-optic noise, respectively. We also consider the effect in which power from the laser beam is absorbed into the mirror, which gives rise to photothermal noise.

2.1. Brownian noise

For a particular material, mechanical loss is quantified by the material's loss angles, which appear as small imaginary components in the material's elastic moduli. In the case of an isotropic material[7], the bulk and shear moduli can be written as $K = K_0(1 + i\phi_B)$ and $\mu = \mu_0(1 + i\phi_S)$, respectively, where ϕ_B is the bulk loss angle and ϕ_S is the shear loss angle [21]. When the material is subjected to a sinusoidally varying force $F(t) = F_0 \cos(2\pi ft)$, these loss angles lead to a time-averaged power dissipation $W(f) = 2\pi f(U_B\phi_B + U_S\phi_S)$, where U_B is the maximum energy stored in bulk deformation, and U_S is the maximum energy stored in shear deformation.

According to the fluctuation–dissipation theorem (FDT), mechanical dissipation leads to fluctuation in the generalized coordinate x conjugate to F [22]. Using the 'direct approach' [23, 24], the power spectral density (PSD) of the fluctuations in x is given by

$$S_x(f) = \frac{2k_BT}{\pi^2 f^2} \frac{W(f)}{F_0^2}. \qquad (1)$$

[7] For cubic single crystals, there are three complex elastic constants to consider.

With W computed as above, $S_x(f)$ is the Brownian noise in the material.

2.2. Thermo-optic noise

Thermo-optic noise is a consequence of thermodynamically driven temperature fluctuations within a material. Again using the fluctuation–dissipation theorem, the PSD $S_T(f)$ of temperature fluctuations can be computed by considering the generalized force conjugate to temperature; namely, the entropy [25]. With $S_T(f)$ in hand, the thermo-optic contribution to the cavity length noise $S_L(f)$ can be computed via the CTE $\alpha = (1/L)\partial L/\partial T$ (giving thermoelastic noise, with PSD $S_x^{(TE)}$) and the CTR $\beta = \partial n/\partial T$ (giving thermorefractive noise, with PSD $S_x^{(TR)}$) [19, 26].

2.3. Photothermal noise

The coefficients of thermal expansion and thermorefraction can manifest themselves not only through thermo-optic noise, but also through photothermal noise, in which laser power is absorbed in the coating and subsequently produces fluctuations in the coating's temperature. In the frequency band of interest, the thermodynamic fluctuations and the laser power fluctuations have thermal lengths which are much larger than the coating thickness. Therefore, the coherent cancellation of the thermodynamically induced thermoelastic and thermorefractive noises will also occur for the noises induced by laser power fluctuation (i.e. the photothermal noise). Since the level of photothermal noise is proportional to the absorbed power, its effect can be enhanced for observation by modulating the power incident on the mirrors. By observing the cancellation of photothermal noise, we can use it as evidence for the cancellation of thermo-optic noise. The details on the measurement will be discussed in section 5.

3. Noise budget for Fabry–Pérot cavities with AlGaAs-coated mirrors

The optical, mechanical, and material parameters for our reference cavities are given in table 1. Where two values are given, these refer to the values measured for each of the two cavities.

In this section we give a concise overview of the noise budget for our fixed-spacer Fabry–Pérot cavities. A more detailed explanation of such noise budgeting has already been given by Chalermsongsak *et al* [32].

The length noise $S_L(f)$ of a fixed-spacer cavity is

$$S_L = 2S_x^{(cBr)} + 2S_x^{(cTO)} + 2S_x^{(subBr)} + 2S_x^{(subTE)}$$
$$+ S_L^{(spBr)} + S_L^{(spTE)} + 4S_x^{(PT)}. \qquad (2)$$

3.1. Coating noise

The quantity $S_x^{(cBr)}$ is the effective displacement of each mirror's position due to coating Brownian noise. By treating

Table 1. Parameters for our reference cavities.

Symb.	Description	Value	Notes
L	Nominal spacer length	36.8(3) mm	
R_{sp}	Outer spacer radius	19.0 mm	
r_{sp}	Inner spacer radius	5.1 mm	
R_s	Mirror substrate radius	25.4 mm	
$\mathcal{R}$	Mirror radius of curvature	1000(5) mm	As specified before application of coatings. 0.5% uncertainty assumed.
λ_0	Laser vacuum wavelength	1064 nm	
w	Spot size on mirrors	215.4(5) m	Defined as the radius for which the beam intensity I satisfies $I(w) = I(0)/e^2$. Computed as $w = (\lambda_0 \mathcal{R}/\pi)^{1/2}/(2\mathcal{R}/L - 1)^{1/4}$.
$\mathcal{F}$	Finesse	16 700(1400), 17 600(1600)	From measurement of the cavity poles.
$\mathcal{T}$	Transmissivity (per mirror)	153(7) ppm	Average over five mirrors fabricated for this work.
$\mathcal{A}$	Absorption (per mirror)	4.96(23) ppm, 5.19(27) ppm	From measurement of the photothermal transfer function.
$\mathcal{S}$	Scatter (per mirror)	30(17) ppm, 20(18) ppm	Calculated as $\mathcal{S} = \pi/\mathcal{F} - \mathcal{T} - \mathcal{A}$
T	Cavity temperature	305(1) K	
E_s	Young's modulus of fused silica	72(1) GPa	
σ_s	Poisson's ratio of fused silica	0.170(5)	
κ_s	Thermal conductivity of fused silica	1.38 W (m K)$^{-1}$	
C_s	Heat capacity of fused silica	1.6×10^6 J (m^3 K)$^{-1}$	
α_s	CTE of fused silica	5.1×10^{-7} K^{-1}	
n_s	Refractive index of fused silica	1.46	
ϕ_s	Loss angle of fused silica	1×10^{-7}	
x	Aluminum alloying fraction	0.920(6)	
E_L	Young's modulus of Al$_{0.92}$Ga$_{0.08}$As	100(20) GPa	Nominal value from Cole *et al* [12]. 20% uncertainty assumed.
E_H	Young's modulus of GaAs	100(20) GPa	See note for E_L.
σ_L	Poisson's ratio of Al$_{0.92}$Ga$_{0.08}$As	0.32(3)	After Adachi [27, p. 24]. 10% uncertainty assumed.
σ_H	Poisson's ratio of GaAs	0.32(3)	See note for σ_L.
κ_L	Thermal conductivity of Al$_{0.92}$Ga$_{0.08}$As	70(4) W (m K)$^{-1}$	Computed as $(55 - 212x + 248x^2)$ W m^{-1} K^{-1}, from the Ioffe Institute [28]. 5% uncertainty assumed.
κ_H	Thermal conductivity of GaAs	55(3) W (m K)$^{-1}$	See note for κ_L.
C_L	Heat capacity of Al$_{0.92}$Ga$_{0.08}$As	$1.70(9) \times 10^6$ J (m^3 K)$^{-1}$	Computed as $(1.75 + 0.11x - 0.19x^2) \times 10^6$ J (m^3 K)$^{-1}$, from Adachi [27, p. 41] and the Ioffe Institute [28]. 5% uncertainty assumed.
C_H	Heat capacity of GaAs	$1.75(9) \times 10^6$ J (m^3 K)$^{-1}$	See note for C_L.
α_L	CTE of Al$_{0.92}$Ga$_{0.08}$As	$5.2(3) \times 10^{-6}$ K^{-1}	Computed as $(5.73 - 0.53x) \times 10^{-6}$ K^{-1}, after Levinshtein *et al* [29, p. 4]. 5% uncertainty assumed.
α_H	CTE of GaAs	$5.7(3) \times 10^{-6}$ K^{-1}	See note for α_L.
β_L	CTR of Al$_{0.92}$Ga$_{0.08}$As	$179(7) \times 10^{-6}$ K^{-1}	Computed as $[366(7) - 203x] \times 10^{-6}$ K^{-1}, after measurements on GaAs and AlAs by Talghader and Smith [30, 31].
β_H	CTR of GaAs	$366(7) \times 10^{-6}$ K^{-1}	See note for β_L.
n_L	Refractive index of Al$_{0.92}$Ga$_{0.08}$As	2.98(3)	After Cole *et al* [12]. 1% uncertainty assumed.
n_H	Refractive index of GaAs	3.48(3)	See note for n_L.
α_c	Effective CTE of coating	$19(3) \times 10^{-6}$ K^{-1}	Computed in appendix B
β_c	Effective CTR of coating	$79(4) \times 10^{-6}$ K^{-1}	Computed in appendix B
C_c	Effective heat capacity of coating	$1.73(6) \times 10^6$ J (m^3 K)$^{-1}$	Computed in appendix B
κ_c	Effective thermal conductivity of coating	61.6(2.4) W (m K)$^{-1}$	Computed in appendix B
N	Number of coating layers	57	
d	Total thickness of coating	4.6806(4) m	Physical thickness, assuming 50 pm random uncertainty in each layer. There is additional systematic uncertainty; see appendix A.
ϕ_c	Effective coating loss angle	$2.41(20) \times 10^{-5}$	From ringdown measurements by Cole *et al* on QWL AlGaAs microresonators [14].

Note: From the Ioffe Institute, the density of Al$_{0.92}$Ga$_{0.08}$As is $\rho = (5.32 - 1.56x) \times 10^3$ kg m^{-3}. From Adachi, the specific heat capacity is $\mathcal{C} = (320 + 132x)$ J (kg K)$^{-1}$. The volumetric heat capacity is then $C = \mathcal{C}\rho$.

the coating as a thin, homogeneous layer of material with a Young's modulus E_c and a Poisson's ratio σ_c, one can write this noise as [12]

$$S_x^{(cBr)}(f) = \frac{2k_BT}{\pi^2 f} \frac{d}{w^2 E_s^2} \frac{\phi_c}{E_c(1-\sigma_c^2)} \times [E_c^2(1+\sigma_s)^2(1-2\sigma_s)^2$$
$$+ E_s^2(1+\sigma_c)^2(1-2\sigma_c)], \quad (3)$$

where ϕ_c is the coating's loss angle. This loss angle is a linear combination of the bulk and shear loss angles of the individual coating materials.

The quantity $S_x^{(cTO)}$ is the effective displacement of each mirror's position due to coating thermo-optic noise [19]:

$$S_x^{(cTO)}(f) = S_T(f)\,\Gamma_{tc}(f)\,(\alpha_c d - \beta_c\lambda_0 - \alpha_s dC_c/C_s)^2, \quad (4)$$

with [33, equations (3.27)–(8)]

$$S_T(f) = \frac{2^{3/2}k_BT^2}{\pi\kappa_s w}M(f/f_T), \quad (5)$$

where $f_T = \kappa_c/(\pi w^2 C_c)$ and

$$M(\Omega) = \int_0^\infty du\, \text{Re}\left[\frac{u\,e^{-u^2/2}}{(u^2 - i\,\Omega)^{1/2}}\right]. \quad (6)$$

Γ_{tc} is a correction factor accounting for the nonzero thickness of the coating [19, equation (39)].

The optimized structure of our coatings results in thermo-optic noise whose PSD $S_x^{(cTO)}$ is lower than the incoherent sum $S_x^{(cTE)} + S_x^{(cTR)}$ of the thermoelastic and thermorefractive noise terms (the first two terms of equation (4), respectively). In figure 1 we plot the anticipated thermo-optic, thermoelastic, thermorefractive, and Brownian noises of our coatings, along with the same noises for a hypothetical 57-layer QWL coating whose first and last layers are GaAs.

3.2. Substrate and spacer noise

By computing the substrate thermoelastic noise $S_r^{(subTE)}$ following Cerdonio *et al* [34], we anticipate that $S_x^{(subTE)}$ will be a limiting noise source for our cavities below 100 Hz. Additionally, we have analytically computed the substrate Brownian noise $S_x^{(subBr)}$ following Levin [24, equation (2)] and Liu *et al* [35, equation (59)], and have found that this noise is much less than the coating Brownian noise at all frequencies of interest. In the case of the spacers, we used a finite-element model to compute the Brownian and thermo-elastic noises, and have found them to be negligible as well. For details, we again refer the reader to the full discussion in Chalermsongsak *et al* [32]. In the rest of this work, we only consider the thermal noise mechanisms arising from the coatings, and from the thermoelastic noise of the fused silica substrates.

3.3. Photothermal noise

The quantity $S_x^{(PT)}$ is the effective displacement of each mirror's position due to photothermal noise:
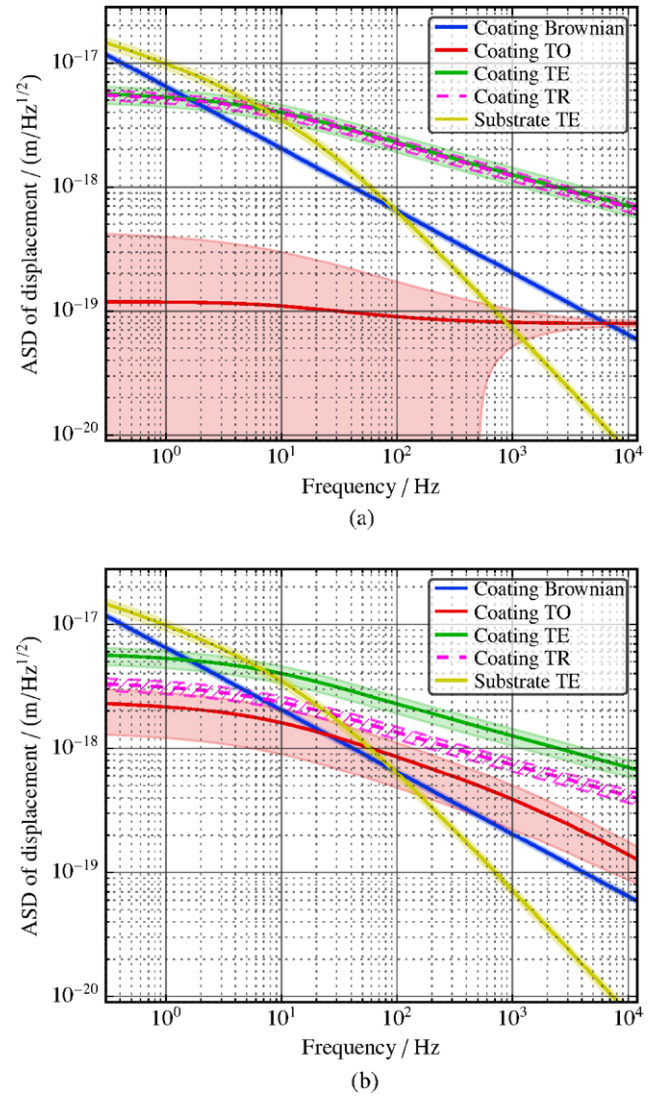

Figure 1. Important thermal noise sources for our optimized AlGaAs mirrors (figure 1(a)) and for a 57-layer QWL stack (figure 1(b)). The shaded/hatched regions indicate 1σ uncertainties propagated forward from the uncertainties given in table 1. Our optimized coatings are designed to maximize the cancellation between the TE and TR noise terms, resulting in TO noise that is subdominant to the coating Brownian and substrate thermoelastic noises below 5 kHz. (a) Anticipated thermal noise sources for our optimized AlGaAs mirrors. (b) Thermal noise sources for a hypothetical 57-layer QWL coating, with the first and last layers being GaAs.

$$S_x^{(PT)}(f) = \left|H^{(PT)}(f)\right|^2 S_P(f), \quad (7)$$

where $H^{(PT)}(f)$ is the photothermal transfer function which takes intracavity power fluctuation $P(f) = P_0/(1 + if/f_{cav})$ to displacement $x(f)$. It has coating thermoelastic, coating thermorefractive, and substrate thermoelastic contributions which are described in detail by Farsi *et al* [36, appendix A]:

$$H^{(PT)}(f) = H^{(cTE)}(f) + H^{(cTR)}(f) + H^{(sTE)}(f). \quad (8)$$

The noise $S_x^{(PT)}(f)$ enters into equation (2) with a factor of 4 because the photothermal fluctuations in the two mirrors are driven coherently by the field circulating in the cavity.

By applying the formalism of Farsi *et al* to our coating design[8], we anticipate that our coatings should display coherent cancellation of $H^{(\text{cTE})}$ and $H^{(\text{cTR})}$. In figure 5 we plot the expected photothermal transfer function of our coatings.

4. Optimization of coating structure

Examining equation (4), it is evident that the thermo-optic noise can be nearly cancelled by manufacturing a mirror whose material parameters satisfy $(\alpha_c - \alpha_s C_c/C_s)d = \beta_c \lambda_0$.

In designing our AlGaAs Bragg mirrors, we wanted a layer structure that would produce a coating with (1) minimal thermo-optic noise $S_x^{(\text{cTO})}$ in our band of interest (10 Hz–1 kHz), (2) a transmissivity $\mathcal{T}$ close to our target $\mathcal{T}_0 = 200$ ppm, and (3) a reflected phase Δ that is close to $\Delta_0 = 180°$. To that end, we constructed an initial cost function

$$y\left[S_x^{(\text{cTO})}(f_0), \mathcal{T}, \Delta\right] = w_1 S_x^{(\text{cTO})}(f_0) + w_2 \left(\frac{\mathcal{T} - \mathcal{T}_0}{\mathcal{T}_0}\right)^2 + w_3 (\Delta - \Delta_0)^2,$$
(9)

where w_1, w_2, and w_3 are weights, and $f_0 = 100$ Hz[9]. The quantities $S_x^{(\text{cTO})}(f_0)$, $\mathcal{T}$, and Δ are functions of the layer structure $\mathbf{d} = (d_1 \quad d_2 \quad d_3 \quad \cdots \quad d_{57})^T$.

Then, to ensure that our optimization was robust against small uncertainties in the indices of refraction n_L and n_H, we constructed a modified cost function:

$$y' = \sum_{n_H} \sum_{n_L} y\left[S_x^{(\text{cTO})}(f_0), \mathcal{T}, \Delta; n_H, n_L\right]$$
(10)

with $n_H \in \{3.47, 3.50, 3.53\}$ and $n_L \in \{2.97, 3.00, 3.03\}$. We then numerically minimized this cost function in order to find an optimal layer structure $\mathbf{d}$.

To test the robustness of our layer structure against other material parameters, we ran a Monte Carlo simulation using the parameter values and uncertainties for the heat capacities, thermal conductivities, Young's moduli, Poisson's ratios, CTEs, and CTRs of GaAs and $Al_{0.92}Ga_{0.08}As$. We also took into account possible systematic and statistical errors in the thickness of each coating layer. The simulation shows that 70% of the trials result in coatings that satisfy (1) $\sqrt{S_x^{(\text{cTO})}(f_0)} < 3.9 \times 10^{-20}$ m Hz$^{-1/2}$, (2) 100 ppm $< \mathcal{T} < 300$ ppm, and (3) $|\Delta - 180°| < 7°$.

In figure 2, we plot the structure of our optimized AlGaAs coating. The numerical values for each coating layer are given in table A1 in the appendix A. In figure 3 we plot the expected performance of our optimized structure as a function of n_L and n_H.

5. Experiment

A diagram of the experiment is shown in figure 4. This setup has been described in detail previously [32]; we briefly summarize the salient points here.

---

[8] In the formalism of Farsi *et al*, the relevant coating CTE is a simple volumetric average $\alpha_c' = \sum_j \alpha_j d_j/d$ rather than the CTE α_c presented in appendix B of this work.
[9] The condition $\Delta_0 = 180°$ ensures that the field at the surface of the coating is nearly zero. This reduces the likelihood that contaminants such as dust will be burned onto the coating [43, section 5.2.2].
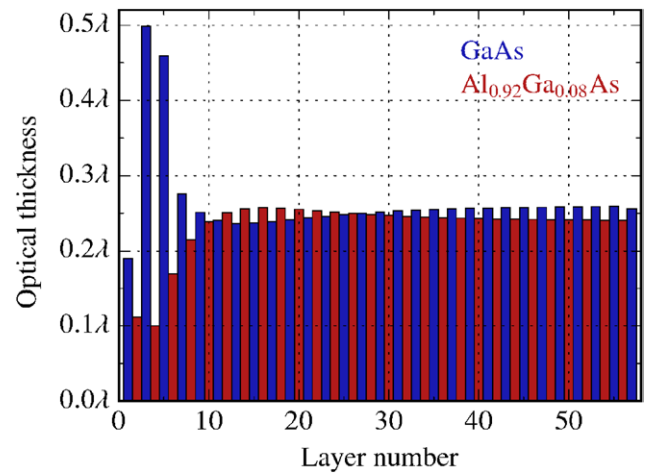

Figure 2. Optimized layer structure of our AlGaAs coatings. Each layer is expressed in optical thickness, so that $\lambda = \lambda_0/n_L$ for the low-index ($Al_{0.92}Ga_{0.08}As$) layers and $\lambda = \lambda_0/n_H$ for the high-index (GaAs) layers.

We independently lock a 1064 nm non-planar ring oscillator (NPRO) laser to each cavity. We use the Pound–Drever–Hall interrogation technique [37, 38] to derive an error signal which indicates the detuning of the laser from cavity resonance. This error signal is electronically amplified and filtered to produce a control signal. At frequencies from DC to tens of kilohertz, this control voltage is applied to a piezoelectric transducer (PZT) attached to the NPRO crystal. At frequencies from tens to hundreds of kilohertz, the control voltage is applied to a broadband, MgO:LiNbO$_3$ electro-optic modulator (EOM). This servo loop achieves a unity-gain frequency above 700 kHz. Within the bandwidth of the servo, the laser frequency is made to tightly track the length fluctuation of the cavity.

The transmitted beams from the two cavities are interfered on an RF photodiode, producing an RF beat note with a frequency $\nu_b = \nu_2 - \nu_1$ of approximately 10 MHz. Using a voltage-controlled oscillator (VCO) of similar frequency, we form a high-gain phase-locked loop (PLL). The control signal of this PLL is proportional to the differential frequency fluctuations of the two cavities.

The experiment is additionally equipped with an intensity stabilization servo (ISS). For each cavity, a portion of the transmitted beam is directed onto a large-area photodiode. The resulting audio-band signal is amplified and fed back to an electro-optic amplitude modulator (EOAM), thereby stabilizing the cavity power in the frequency band of interest.

6. Results

6.1. Photothermal transfer function

For each cavity, we measured the photothermal transfer function as follows. With the ISS disengaged, we drove the EOAM with a sinusoidal voltage $V(f)$. We then measured the transfer function which takes the transmitted cavity power $P_{\text{trans}}(f)$ (measured via a calibrated photodiode) to beat note fluctuation $\nu_b(f)$. The measured transfer function $\nu_b(f)/P_{\text{trans}}(f)$ can
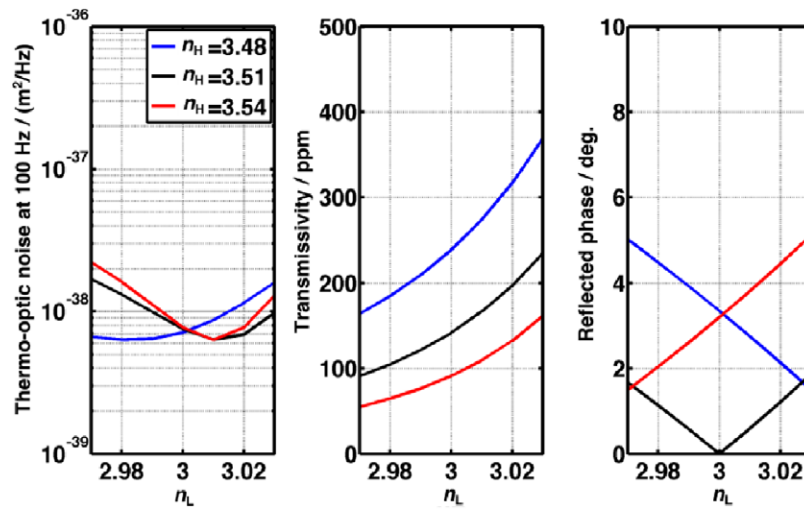
Figure 3. Expected thermo-optic noise (at 100 Hz), transmissivity, and reflection phase (modulo 180°) of our optimized coating, given small uncertainties in n_L and n_H.
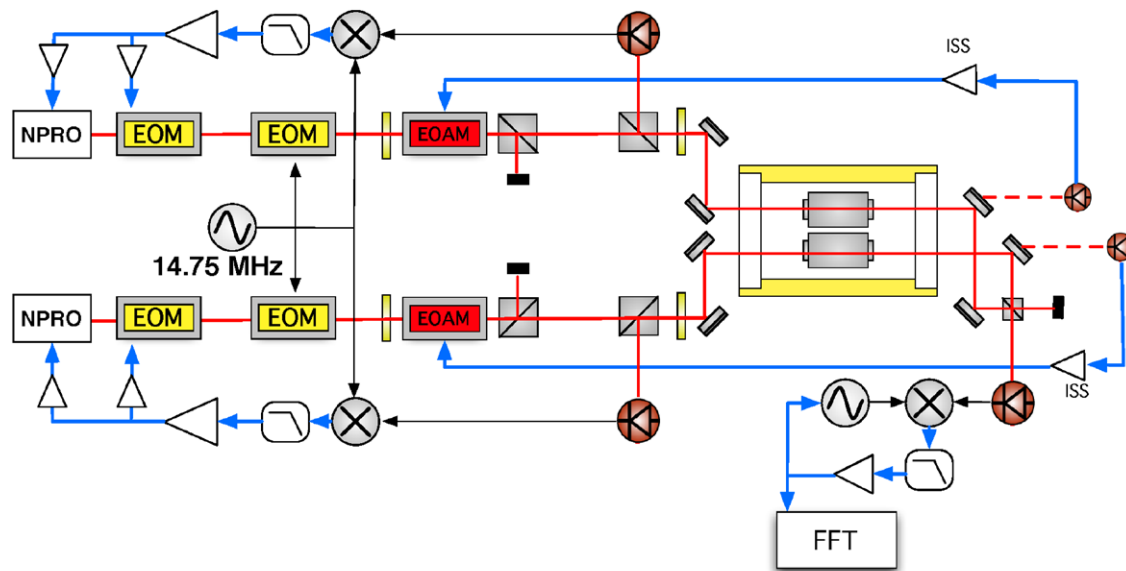

Figure 4. Diagram of experimental setup used to measure the beat note between two 3.68 cm Fabry–Pérot cavities with AlGaAs mirror coatings. The box labeled 'FFT' is an audio-band signal analyzer which is capable of measuring both PSDs and swept-sine transfer functions. Diagram reproduced from figure 4 of Chalermsongsak *et al* [32]. © Bureau International des Poids et Mesures. Reproduced by permission of IOP Publishing.

be used to estimate the per-coating absorption $\mathcal{A}$ by comparing with the expected transfer function $H^{(PT)}(f) = \nu_b(f)/P_{abs}(f)$ in equation (8). Here $P_{abs}(f) = \mathcal{A} P_{circ}(f) = \mathcal{A} P_{trans}(f)/\mathcal{T}$, and $\mathcal{T} = 153(7)$ ppm is the measured per-mirror transmissivity (to be compared to the value of 151 ppm, computed from the nominal coating design).

To obtain an estimate of $\mathcal{A}$, we write our measurement as $\hat{H}^{(PT)}(f) = \mathcal{T}\nu_b(f)/\mathcal{A} P_{trans}(f)$ and then minimize the sum

$$\sum_{f_i \leqslant 10\,\text{Hz}} \left| \log_{10} \frac{\hat{H}^{(PT)}(f_i)}{H^{(PT)}(f_i)} \right|^2 \qquad (11)$$

with respect to $\mathcal{A}$. For each of the cavities, we find mean per-mirror absorptivities of 4.96(1) ppm and 5.19(13) ppm, where the uncertainties are statistical. To these uncertainties we must

add the uncertainty in the value of the transmission $\mathcal{T}$ used to estimate the circulating cavity power. With this uncertainty incorporated, our measured absorptivities are 4.96(23) ppm and 5.19(27) ppm. For our coatings, the penetration depth is $\delta = 560$ nm, and so the absorption coefficient is $\alpha = \mathcal{A}\ l/(2\delta) \sim 0.05\ \text{cm}^{-1}$.

In figure 5 we show the measured photothermal transfer functions for our AlGaAs coatings, along with the expectation. Below 10 Hz, the magnitude and phase agree well with the expectation, particularly for the north cavity. From 10 Hz to 3 kHz, the agreement between measurement and expectation is imperfect, and the cause of the discrepancy at high frequencies is not understood; it may be laser power fluctuation coupling into the PLL. However, it is evident that the measured transfer functions have magnitudes that lie below the individual thermoelastic and thermorefractive contributions to
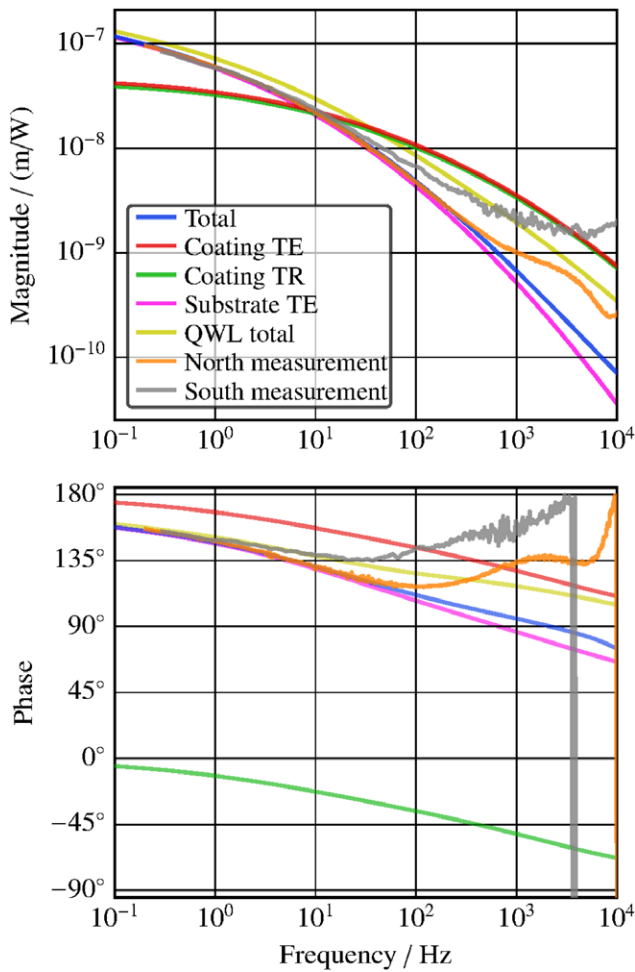
Figure 5. Measured photothermal transfer function, along with expected transfer function after Farsi *et al* [36], for our two cavities (labeled 'north' and 'south'). The units are chosen so that the transfer function takes the absorbed power (per mirror) to the shift in the sensed displacement of each mirror. In this plot we also show the total photothermal transfer function that would be expected from a 57-layer QWL coating, as in figure 1(b).

the expected photothermal transfer function. We take this as strong evidence that thermo-optic cancellation has been successfully realized in these coatings.

6.2. Scatter

To assess the scatter of our AlGaAs coatings, we used the technique described by Magaña-Sandoval *et al* [39] to measure the bidirectional reflectance distribution function (BRDF) of our coatings. With a laser normally incident on the coating, light is scattered into 2π steradians. To measure the scatter, we scan a calibrated CCD camera in altitude (from roughly 15°–75° angle of incidence) and record the number of counts registered. By assuming the scattering is azimuthally symmetric, we compute the BRDF and subsequently the total integrated scatter (TIS) over the sampled altitude. The result for one of our mirrors is shown in figure 6. We found a wide variation in the level of scatter of our coatings, even after several rounds of cleaning. The lowest TIS achieved was 2.7(5) ppm. For two of the other mirrors, we measured TISs of 17.9(1.0) ppm, and
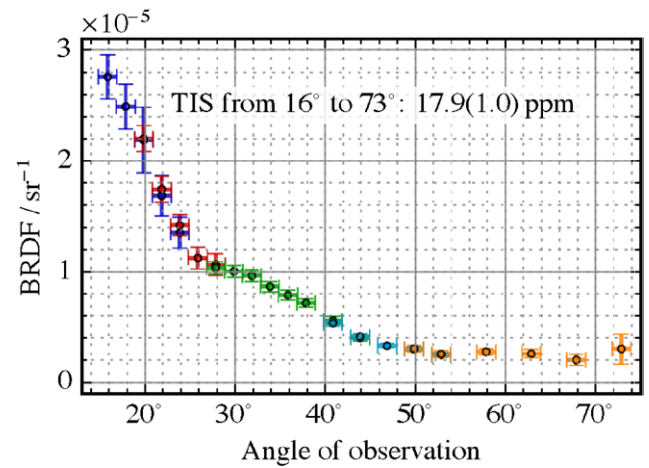

Figure 6. A representative BRDF measurement of our AlGaAs coatings. Different colors denote different exposure times for the CCD acquisition.
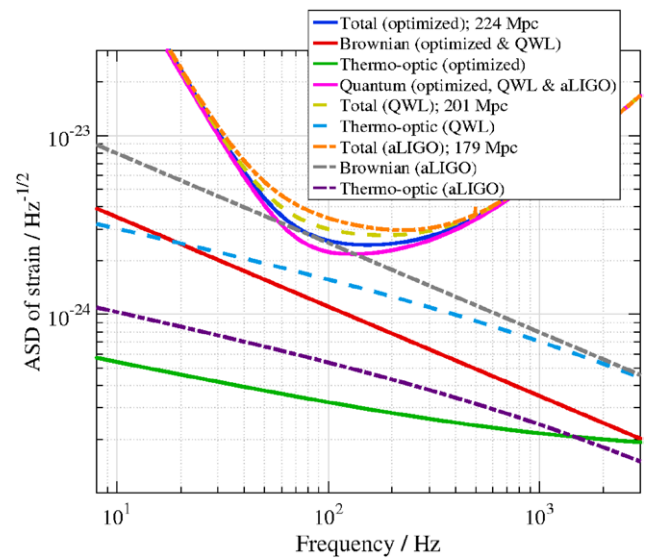

Figure 7. Strain curve for a gravitational wave detector with fused silica test masses coated with optimized AlGaAs coatings. For comparison, the analogous strain curves for QWL AlGaAs coatings, and for silica/tantala coatings, are shown. All other parameters are assumed identical to those of Advanced LIGO.

17.0(1.0) ppm. The TIS of the fourth mirror was not measured after its final cleaning.

The scatter values measured by this method are slightly lower than, but within the errors of, the scatter values given in table 1, which are inferred from the total cavity losses. However, our BRDF measurements did not measure the power scattered at small angles ($<15°$), and will thus underestimate the total scatter.

7. Discussion

7.1. Implications for gravitational wave detectors

Using the method described in section 4, we have carried out a coating optimization for a version of Advanced LIGO in which the test mass coatings are fabricated from

AlGaAs-based crystalline coatings and transferred to fused silica substrates. The optimization was run with 29 layers on each input test mass and 81 layers on each end test mass. In figure 7 we plot the resulting strain curve for such a detector, along with the strain curve for a version of Advanced LIGO with QWL AlGaAs coatings (28 layers on each input test mass, and 78 layers on each end test mass), and the strain curve for Advanced LIGO with as-built titania-doped silica/tantala coatings. Both the optimized coatings and the QWL coatings produce a Brownian noise whose strain ASD is $\sqrt{S^{(\text{cBr})}(f)} = (1.1 \times 10^{-23}\ \text{Hz}^{-1/2}) \times (1\ \text{Hz}\,/f)^{1/2}$, which is more than a factor of 2 below the anticipated ASD for the currently installed silica/tantala coatings. However, our optimized coatings offer superior thermo-optic noise performance across the entire gravitational wave band (10 Hz–7 kHz), compared to the QWL coatings. As a result, the detector's binary neutron star inspiral range [40] increases from 201 Mpc for the QWL coatings to 224 Mpc for the optimized coatings. The anticipated range is 179 Mpc for the silica/tantala coatings.

7.2. Conclusion

We have demonstrated cancellation of photothermal noise in high-reflectivity substrate-transferred AlGaAs coatings. This cancellation was achieved by optimizing the coating layer structure in such a way that the thermo-elastic and thermo-refractive contributions to the thermo-optic noise destructively interfere, hence minimizing the total coating thermo-optic noise. Our result for the per-mirror absorption coefficient ($\alpha = 0.05\ \text{cm}^{-1}$) is consistent with the result of Steinlechner *et al* [41], who used photothermal common-path interferometry on a set of QWL AlGaAs high-reflectors to arrive at an absorption coefficient of $0.06\ \text{cm}^{-1}$.

The measured absorption and scatter from these coatings are promising, but improvement in the optical performance will be required for use in future gravitational wave interferometers. For Advanced LIGO, requirements for scatter and absorption are set at the few-ppm and sub-ppm level, respectively [8], and the requirements for third-generation interferometers may be even more stringent. Additionally, for kilometer-scale interferometers, the spot sizes on the test masses can be more than 5 cm. This requires coating diameters which are tens of centimeters in diameter in order to avoid significant clipping losses of the beam. In order for these coatings to be viable for gravitational wave detectors, the substrate transfer process must be scaled up by more than a factor of 10 in diameter.

Acknowledgments

Appendix A. Coating structure

In table A1 we give the thickness of each layer of our AlGaAs coatings, in terms of optical thickness d_j/λ_j. For each layer, the physical thickness d_j can only be controlled to the nearest 50 pm. Additionally, there is systematic error in the thickness control for the GaAs and $Al_{0.92}Ga_{0.08}As$ layers; the fractional uncertainties for this error are 0.5% and 1.0%, respectively.

Appendix B. Thermo-optic material parameters

The effective CTE of the coating is [19, equations (A1)–(A3)]

$$\alpha_c = \sum_{j=1}^{N} \alpha_j\, \frac{d_j}{d}\, \frac{1+\sigma_s}{1-\sigma_j}\left[\frac{1+\sigma_j}{1+\sigma_s} + (1-2\sigma_s)\frac{E_j}{E_s}\right], \quad \text{(B.1)}$$

the effective CTR of the coating is

$$\beta_c = -\frac{1}{\lambda_0}\frac{\partial x^{(\text{TR})}}{\partial T}. \quad \text{(B.2)}$$

where $x^{(\text{TR})}$ is the change in the sensed mirror position due to thermorefractive effects. For a coating made entirely of QWL structure with high index material (n_H) as a top layer, β_c can be approximated by [18, equation (A.14)]

$$\beta_c \approx \frac{B_H + B_L}{4(n_H^2 - n_L^2)}, \quad \text{(B.3)}$$

where B_X is the fractional change in optical path length with respect to temperature in material X [42, equation (31)][10]:

$$B_X = \beta_X + n_X\alpha_X\frac{1+\sigma_X}{1-\sigma_X}. \quad \text{(B.4)}$$

The effective heat capacity of the coating is [19, equation (A4)]

---

[10] The value for B_X here follows the calculation laid out by Yamamoto [42], which is slightly different from what is used by Evans *et al* [19, equations (A1), (B8) and (B15)]. Since thermorefractive noise arises from the phase shift of the beam propagating back and forth inside the coating, the imaginary force used in the direct approach has to be applied on both sides of the coating. Thus, the deformation in the coating is not related to the substrate, and the effective thermal expansion is only corrected by the Poisson ratio of the coating. All calculations and optimizations done in this work use this notion for B_X.

Table A1. Optical thickness of each coating layer, in fractions of a wavelength.

Layer	d_j/λ_j				
1–5	0.1896	0.1121	0.4995	0.1000	0.4598
6–10	0.1695	0.2760	0.2145	0.2510	0.2388
11–15	0.2403	0.2508	0.2368	0.2553	0.2375
16–20	0.2571	0.2391	0.2564	0.2414	0.2550
21–25	0.2437	0.2533	0.2459	0.2515	0.2480
26–30	0.2498	0.2498	0.2482	0.2514	0.2469
31–35	0.2528	0.2457	0.2539	0.2447	0.2549
36–40	0.2439	0.2556	0.2433	0.2562	0.2427
41–45	0.2566	0.2423	0.2571	0.2420	0.2574
46–50	0.2417	0.2577	0.2414	0.2579	0.2412
51–55	0.2581	0.2409	0.2585	0.2405	0.2587
56–57	0.2401	0.2556			

Note: Odd-numbered layers are GaAs ($n_H = 3.51$), and even-numbered layers are Al$_{0.92}$Ga$_{0.08}$As ($n_L = 3.00$).

$$C_c = \sum_{j=1}^{N} C_j \frac{d_j}{d}. \tag{B.5}$$

The effective thermal conductivity of the coating is

$$\kappa_c = \left(\sum_{j=1}^{N} \frac{1}{\kappa_j} \frac{d_j}{d} \right)^{-1}. \tag{B.6}$$

References

[1] The LIGO Scientific Collaboration 2015 *Class. Quantum Grav.* **32** 074001
[2] Zhang W *et al* 2014 *Opt. Lett.* **39** 1980
[3] Chen L, Hall J L, Ye J, Yang T, Zang E and Li T 2006 *Phys. Rev.* A **74** 053801
[4] Ludlow A D, Huang X, Notcutt M, Zanon-Willette T, Foreman S M, Boyd M M, Blatt S and Ye J 2007 *Opt. Lett.* **32** 641
[5] Alnis J, Matveev A, Kolachevsky N, Udem T and Hänsch T W 2008 *Phys. Rev.* A **77** 053809
[6] Harry G M and the LIGO Scientific Collaboration 2010 *Class. Quantum Grav.* **27** 084006
[7] Penn S D *et al* 2003 *Class. Quantum Grav.* **20** 2917
[8] Harry G M *et al* 2007 *Class. Quantum Grav.* **24** 405
[9] Villar A E *et al* 2010 *Phys. Rev.* D **81** 122001
[10] Yam W, Gras S and Evans M 2015 *Phys. Rev.* D **91** 042002
[11] Steinlechner J, Martin I W, Hough J, Krüger C, Rowan S and Schnabel R 2015 *Phys. Rev.* D **91** 042001
[12] Cole G D, Zhang W, Martin M J, Ye J and Aspelmeyer M 2013 *Nat. Photon.* **7** 644
[13] Cole G D, Bai Y, Aspelmeyer M and Fitzgerald E A 2010 *Appl. Phys. Lett.* **96** 261102
[14] Cole G D, Wilson-Rae I, Werbach K, Vanner M R and Aspelmeyer M 2011 *Nat. Commun.* **2** 231
[15] Cole G D 2012 *Proc. SPIE* **8458** 845807
[16] van der Ziel J P and Ilegems M 1975 *Appl. Opt.* **14** 2627
[17] Jewell J L, Scherer A, McCall S L, Gossard A C and English J H 1987 *Appl. Phys. Lett.* **51** 94
[18] Gorodetsky M L 2008 *Phys. Lett.* A **372** 6813
[19] Evans M, Ballmer S, Fejer M, Fritschel P, Harry G and Ogin G 2008 *Phys. Rev.* D **78** 102003
[20] Kimble H J, Lev B L and Ye J 2008 *Phys. Rev. Lett.* **101** 260602
[21] Hong T, Yang H, Gustafson E K, Adhikari R X and Chen Y 2013 *Phys. Rev.* D **87** 082001
[22] Callen H B and Welton T A 1951 *Phys. Rev.* **83** 34–40
[23] González G I and Saulson P R 1994 *J. Acoust. Soc. Am.* **96** 207
[24] Levin Y 1998 *Phys. Rev.* D **57** 659
[25] Levin Y 2008 *Phys. Lett.* A **372** 1941
[26] Ballmer S W 2015 *Phys. Rev.* D **91** 023010
[27] Adachi S (ed) 1993 *Properties of Aluminium Gallium Arsenide* (*EMIS Datareviews Series*) (London: Institution of Electrical Engineers)
[28] Ioffe Institute *Aluminum Gallium Arsenide (AlGaAs): Thermal Properties* (http://www.ioffe.ru/SVA/NSM/Semicond/AlGaAs/basic.html)
[29] Levinshtein M, Rumyanstev S and Shur M S 1996 *Handbook Series on Semiconductor Parameters* (*Ternary and Quaternary III-V Compounds* vol 2) (Singapore: World Scientific)
[30] Talghader J and Smith J S 1995 *Appl. Phys. Lett.* **66** 335
[31] Talghader J and Smith J S 1996 *Appl. Phys. Lett.* **69** 2608
[32] Chalermsongsak T, Seifert F, Hall E D, Arai K, Gustafson E K and Adhikari R X 2015 *Metrologia* **52** 17
[33] Martin M J 2013 Quantum metrology and many-body physics: pushing the frontier of the optical lattice clock *PhD Thesis* University of Colorado
[34] Cerdonio M, Conti L, Heidmann A and Pinard M 2001 *Phys. Rev.* D **63** 082003
[35] Liu Y T and Thorne K S 2000 *Phys. Rev.* D **62** 122002
[36] Farsi A, de Cumis M S, Marino F and Marin F 2012 *J. Appl. Phys.* **111** 043101
[37] Drever R, Hall J, Kowalski F, Hough J, Ford G, Munley A and Ward H 1983 *Appl. Phys.* B **31** 97
[38] Hils D and Hall J L 1987 *Rev. Sci. Instrum.* **58** 1406
[39] Magaña-Sandoval F, Adhikari R X, Frolov V, Harms J, Lee J, Sankar S, Saulson P R and Smith J R 2012 *J. Opt. Soc. Am.* A **29** 1722
[40] Sutton P J 2013 ArXiv e-prints
[41] Steinlechner J, Martin I W, Bell A, Cole G, Hough J, Penn S, Rowan S and Steinlechner S 2015 *Class. Quantum Grav.* **32** 105008
[42] Yamamoto K 2013 Thermo-optic noise at cryogenic temperature *Technical Report* No. JGW-T1001852-v1 University of Tokyo
[43] Chalermsongsak T 2014 High fidelity probe and mitigation of mirror thermal fluctuations *PhD Thesis* California Institute of Technology